Available online at www.sciencedirect.com
SCIENCE DIRECT®
Colloids and Surfaces B: Biointerfaces 35 (2004) 159–167
COLLOIDS AND SURFACES B
www.elsevier.com/locate/colsurfb

A dynamic wicking technique for determining the effective pore radius of pregelatinized starch sheets

E.P. Kalogianni [a], T. Savopoulos [a], T.D. Karapantsios [a,b,*], S.N. Raphaelides [a]

[a] *Food Process Engineering Laboratory, Department of Food Technology, Technological Institution of Thessaloniki, P.O. Box 14561, 54101 Thessaloniki, Greece*
[b] *Department of Chemistry, Division of Chemical Technology, Aristotle University of Thessaloniki, University Box 116, 54124 Thessaloniki, Greece*

Accepted 2 March 2004

Abstract

A dynamic wicking technique is employed for the first time for the determination of the effective mean pore radius of a thin-layer porous food: drum dried pregelatinized starch sheets. The technique consists of measuring the penetration rate of various *n*-alkanes in the porous matrix of the starch sheets and using this data to calculate the effective pore radius via the Washburn equation. Pore sizes in the order of a few nanometers have been determined in the starch sheets depending on the drum dryer's operating variables (drum rotation speed, steam pressure and starch feed concentration). The conditions for the application of the technique in porous foods are discussed as compared to the conditions for single capillaries and inorganic porous material measured in other studies.

Keywords: Drum dryer; Porosity; Pore sizes; Wettability; Capillary rise; Washburn equation

1. Introduction

Porous foods in the form of dried agricultural products, cereal products (cookies, bread, extruded foods, breakfast cereals) dried soups, milk powder or other powders used as food additives (e.g. modified starch), constitute a big part of the food industry. The porous structure of foods affects their attributes and functionality while special attention must be paid to its influence on the transport properties of liquids and gases inside the food matrix. These properties control processes such as removal of moisture when the food is dried or cooked (but also its rehydration) as well as diffusion of vapors and gases responsible for the shelf life of some products (e.g. [1–3]). The internal porous network of foods influences also their mechanical strength and texture (e.g. [4]). The in-depth investigation of the porous structure of foods will assist the improvement of already existing foods or allow the development of novel functional foods but will also shed light in the underlying mass and heat transport phenomena during processing.

Porous structures resulting from physical processes during food production, e.g. drying, exhibit a complicated stochastic nature characterized by vacant spaces of various shapes and sizes that deploy and interconnect randomly in three dimensions. It is impossible to describe in detail such a complex structure. The most common quantity used to characterize the internal porous structure in foods is *bulk porosity* (e.g. [5,6]), defined as the volume occupied by the pores versus the total volume of the product. Various methods have been proposed for bulk porosity measurement in foods (e.g. [7,8]). It must be stressed, however, that bulk porosity gives only global information of porous media while a more detailed knowledge of the internal features of the porous matrix is usually needed.

Optical microscopy and microphotography combined with image analysis have been traditionally used in the past to characterize large pores and openings in food products (e.g. [5,9]). Scanning electron microscopy (SEM) has been used to observe much smaller structures (e.g. [9,10]). Optical microscopy and microphotography can give gross information on morphological features such as surface

* Corresponding author. Tel.: +30-2310-99-7772; fax: +30-2310-99-7759.
E-mail address: karapant@chem.auth.gr (T.D. Karapantsios).

0927-7765/$ – see front matter © 2004 Elsevier B.V. All rights reserved.
doi:10.1016/j.colsurfb.2004.03.008

pores shape and size but cannot give reliable information about pores length in three-dimensional networks, pore size distributions and tortuosity [11]. On the other hand, SEM can resolve features down to a very small scale (in the order of few tenths of nm) but it is often difficult to apply it to delicate products such as foods. For such items, the possibility always exists that artifacts may be introduced due to the number of processing steps that the specimen is subjected to before SEM exposure [11]. Evidently, SEM snapshots cannot provide global information about pore size distributions and tortuosity.

A standard technique to characterize porous networks in materials is mercury intrusion porosimetry (MIP). It can be used to determine pores radii (from a few nm to about 100 μm), pore size distributions and pore volumes. This technique has been employed by some authors for the characterization of porous foods [6,3,12,13]. Yet, MIP is a rather expensive technique, requiring special equipment and expertise. Moreover, mercury being a high energy liquid is very susceptible to contamination by impurities embedded in food systems resulting in significant reduction in surface tension and contact angle, a fact that affects drastically the determination of pores characteristics [14].

In this work, a dynamic wicking technique is used for the determination of the effective pore radius in foods. This is an easy to perform technique, needing no expensive equipment or particular expertise. The technique relies on describing liquid penetration kinetics inside a thin layer of a material by the Lucas–Washburn equation (1). The technique has been so far quite popular in studying the porous structure of several inorganic materials and synthetic polymers (e.g. [15–20]). Nevertheless, to the best of our knowledge there is no prior application of this technique to food products.

In the wicking technique, liquids that can penetrate spontaneously into the capillaries of the porous solid are used and the effective pore radius of the medium as well as the contact angle between the porous medium and the liquid can be determined. The determination of the effective pore radius is of interest in this study. When the penetration occurs on the horizontal plane then the rate of penetration can be described by the Lucas–Washburn equation [21]:

$$\frac{h^2}{t} = \frac{r\gamma\cos\theta}{2\eta} \tag{1}$$

where h is the distance traveled by the liquid, t the corresponding rime, r the capillary radius, γ the surface tension of the liquid, θ the liquid–solid contact angle and η the viscosity of the liquid. For porous media, r stands for the effective pore radius. The Lucas–Washburn equation is derived by combining the Poiseuille's law for viscous flow and the Young–Laplace equation for capillarity. The basic conditions for Eq. (1) to be valid are that laminar flow conditions must prevail in the pores (the Reynolds number must be below ∼1200) and that the liquid meniscus must be roughly hemispherical [22]. Furthermore, an adsorbed film of the penetrating liquid needs to preexist in the porous body otherwise an additional driving force arises for liquid spreading due to the free energy reduction of the solid in the process of the adsorbed film formation [16,23].

When penetration occurs on the vertical plane, it is soon influenced by gravity and the penetration rate gradually drops as the height of the liquid increases. Eventually, equilibrium between hydrostatic and capillary pressure is reached at a height h_{eq}:

$$h_{eq} = \frac{2\gamma\cos\theta}{rg\rho} \tag{2}$$

where g is the acceleration of gravity and ρ the liquid density. When $h \ll h_{eq}$, gravity effects can be ignored and the Lucas–Washburn equation describes adequately the capillary rise.

The technique consists of measuring the wicking rate (h^2/t) of wetting liquids in the porous medium. A wetting liquid is one that forms a contact angle of less than 90° with the solid surface. Given the liquid properties, there are two unknowns in Eq. (1), r and $\cos\theta$. The use of alkanes as wetting liquids makes possible the separate determination of r. Alkanes being apolar low energy liquids have an approximately zero contact angle with the solid (so $\cos\theta = 1$) and the only remaining unknown in Eq. (1) is r. In order to calculate r, the customary approach is to plot $2(h^2/t)\eta$ for the various alkanes versus γ [15]. Provided that $\cos\theta = 1$ and that the best-fit line passing through the data and the origin of the plot is linear, the slope of the line yields r. For the reliable application of the technique, the first instants of liquid penetration must be excluded from calculations. This is so because during initial liquid penetration the flow pattern is complex and Poiseuille flow is not respected [15,24–26].

Pregelatinized starches, also referred to as instant starches, are products of drum dryers that in the form of fine powders readily disperse in cold water to form moderately stable pastes [27]. Such products are used mainly as thickeners in foods and as adhesives in foundry core binders and in the textile industry [28]. The purpose of this work was to employ the dynamic wicking technique described by van Oss et al. [15], in characterizing the internal porous network of the thermally modified starches produced by a drum dryer over a useful range of operating conditions. To our knowledge, no systematic study has been conducted in the past on the porous structure of drum dryer products despite its paramount importance for practical applications. In addition, a discussion on some subtle points of the technique when applied to delicate food products is presented.

2. Materials and methods

2.1. Production of pregelatinized starch sheets

Native maize starch was purchased from Group Amylum S.A., Greece. The granules mean diameter was 14.95 μm with a standard deviation of 5.8 μm (measured by a

Malvern MasterSizer, Malvern Instruments Ltd.). A small industrial-scale double drum dryer was employed for the production of pregelatinized maize starch sheets (GOUDA). The drums had 0.5 m diameter and 0.5 m length and were counter-rotating at a rotational speed varied over the range 1–6 rpm. The drums were internally heated by steam at 7 or 8 bar. The level of the liquid pool formed between the upper parts of the closely spaced apart drums was kept at 18 cm. Starch/water suspensions with solids concentration of 7, 10 and 13% (w/w, wet basis) were employed as the dryer feed.

Native starch in suspension with cold water was top-fed to the dryer where it gelatinized first in the pool between the drums of the dryer. A small quantity of this gelatinized material continuously exited through the gap between the drums and dried out in the form of a thin sheet adhered over the hot surfaces of the drums. The produced starch sheets were semi-transparent with a thickness varying approximately between 20 μm (at 7% feed, 6 rpm) and 180 μm (at 13% feed, 1 rpm). That is, the higher feed concentrations and the lower rotational speeds yielded the thicker starch sheets. Apart from being very thin, the produced dry starch sheets were particularly delicate and fragile with a tendency to self wrap-up as a roll when absorbing moisture from the surroundings. So, MIP tests were out of the question.

2.2. Microscopy of the sheets

Drum dryer sheets were examined right after production with an optical microscope at magnifications of 50× and 80×. Photos were also taken by mounting a TTL camera on the microscope ocular lens. Best contrast at the sheet surface was achieved when the samples were illuminated simultaneously from three different angles with the aid of optical fibers (Macrospot 1500, Kaiser).

2.3. Wicking experiments

Drum dryer sheets, cut into straps measuring 1 cm × 3 cm, were fixed at their upper edge to a glass slide (with a small dot of glue), as also done by Li et al. [14]. The 1 cm width of the strap proved adequate to average minor spatial inhomogeneities across the samples whereas a 3 cm length was more than enough to achieve steady penetration rates, yet short enough to avoid gravity effects. The glass slides and glue did not come in contact with the wicking liquid, their role was solely to help handling and suspending the fragile samples. The samples were first dried for 1 h at 130 °C and were then placed for 24 h (minimum) in a desiccator in the presence of vapors of the wicking liquid in order to allow vapors to flood the internal porous network till saturation. Because of the hygroscopic nature of dry starch, the wicking experiments were conducted inside a closed optical glass box (5 cm × 5 cm × 5 cm, Fischer Scientific) containing dry silica gel. Fig. 1 shows schematically the experimental setup.

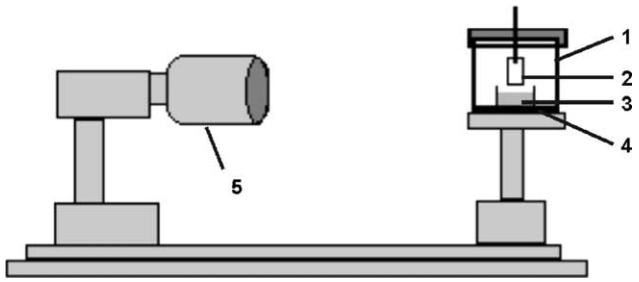

Fig. 1. Experimental setup used for wicking: (1) closed optical glass box; (2) starch sheet; (3) wicking liquid; (4) silica gel; (5) CCD camera.

The advancement of the front of the wicking liquid was observed by a CCD video camera (XC-73CE, Sony) interfaced to a PC. Images were recorded at a predetermined rate that could be adjusted from 1 frame/min up to 1 frame/40 ms. The usual recording rate in this study was 1 frame/s. As with optical microscopy, the samples were illuminated simultaneously from different angles so as to maximize the contrast between the wetted and not wetted areas.

The experiment started by lowering the sample to just touch the free liquid surface in a shallow cap containing the wetting liquid. Fig. 2 presents snapshots from a typical wicking experiment. The contrast between wetted and not wetted zones was intense and the position of the moving front could be easily determined in the recorded images. In almost all cases, the liquid rose into the starch sheet as a flat front. This served also as an independent check of the spatial homogeneity of the porous network across the starch sample. Each drum dryer product was wicked

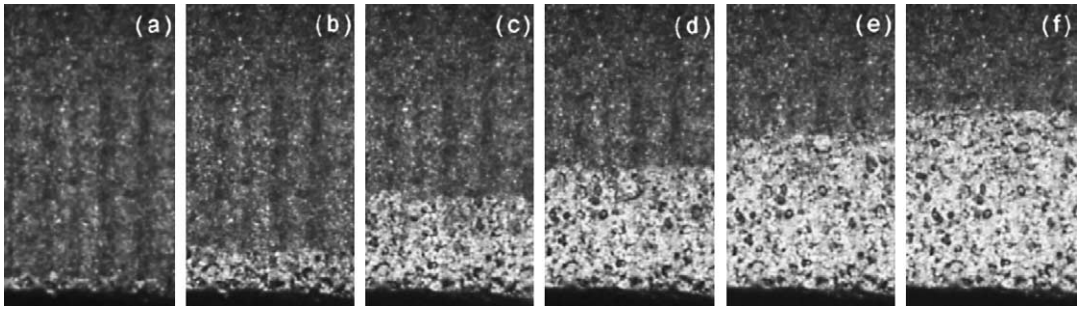

Fig. 2. Wicking of a drum dryer modified starch sheet with decane at: (a) 1 s; (b) 10 s; (c) 50 s; (d) 120 s; (e) 270 s; (f) 400 s. Drum dryer input variables: starch feed concentration, 13%; steam pressure, 8 bar; drum rotation speed, 1 rpm.

Table 1
Viscosity (n) and surface tension (γ) values used for data reduction [29]

Wicking liquids	Viscosity (η, mPa s) (at 25 °C)	Surface tension (γ, mN/m) (at 25 °C)
Pentane	0.274	15.80
Heptane	0.387	19.90
Octane	0.508	21.00
Decane	0.838	23.45
Dodecane	1.383	24.85
Tetradecane	1.724	26.05
Hexadecane	3.032	26.95

with all of the following liquids: *n*-heptane (J.T. Baker, >99%), *n*-octane (Sigma, about >99%), *n*-decane (Sigma, >99%), *n*-dodecane (Sigma, >99%), *n*-tetradecane (Sigma, >98%), *n*-hexadecane (Sigma, >99%). Each sample was used only once for wicking. At least three tests with different samples from the same product were conducted and repeatability was considered satisfactory only if the variance (=S.D./mean) of pore radius measurements was better than 0.2. The first 1–2 mm of wicking were excluded from the analysis because, as already explained, did not follow the Lucas–Washburn equation (1). Experiments were done at 25 ± 1 °C. Data reduction was performed using literature values for the viscosity (η) and surface tension (γ) of the wicking liquids (Table 1).

When wicking was done with the lower molecular weight alkanes (heptane, octane), evaporation from the wetted parts was witnessed as intense local fluctuations in the contrast of these areas. This was also manifested in the plots of h^2 versus t, where a gradually leveling-off curve, instead of a straight line, was found. To overcome evaporation, these two liquids were left inside the glass box for enough time prior to wicking until their vapors saturated the available space. The saturation time of the glass box was determined as the minimum time needed to obtain a straight line when plotting h^2 versus t and it was 48 h for heptane and 72 h for octane (the relatively long times were attributed chiefly to inadequate sealing of the glass box). Tests done with the other liquids (decane, dodecane, tetradecane, hexadecane) gave straight h^2 versus t lines (with no apparent sign of evaporation) even without prior saturation inside the glass box. This is probably due to the low vapor pressure of these liquids at measurement temperatures (more in a subsequent section).

3. Results and discussion

3.1. Morphology of starch sheets: macroscopic observations

In all dried sheets, the granular shape of native starch was completely absent. Instead, the sheets looked like a composite medium in which irregular air pockets (bubbles) and pores were randomly distributed inside the continuous solid phase. It has been reported in the past (e.g. [30,31]) that due to uneven initial deposition of the gelatinized material (exiting the gap between the drums) over the drums surface, the produced sheets exhibit zones with uneven moisture content. Such zones—more evident in the moister sheets—were positively correlated with variations in the local thickness of the sheets [32]. These local variations in moisture and thickness might be responsible for fluctuations in the porosity of the sheet issued during the intense drying process of the sheet around the drums.

Close inspection of the sheets revealed that their appearance was not alike but varied among the different conditions used for production. Sheets produced with 10 and 13% starch feed concentration had two sides of different morphology. The side that was in contact with the surface of the drums was pretty smooth with only few small pores and cracks. The free side of the sheets (in contact with air) was irregular with open cavities or closed air pockets alternating with the continuous solid phase. On the other hand, the sheets produced from suspensions with 7% starch concentration did not present significant differences between the two sides; they were both pretty smooth. Those sheets were the thinnest of all, ~20–60 μm.

3.2. Morphology of starch sheets: microscopic observations

Fig. 3 shows representative microscopy photos of the dry starch sheets under various production conditions. Fig. 3a displays a sheet produced from 13% feed concentration and 1 rpm drum speed. The focus of the optics is on the top (free) surface of the sheet. One can easily observe several open asymmetrical cavities (craters), of about 200–400 μm each, at irregular intervals across the surface of the sheet. Smaller closed air bubbles of about 100–200 μm are spread between these craters. Fig. 3b shows the same sheet as in Fig. 3a but now the focus is at the bottom of the craters. Seemingly, much smaller bubbles (sizes about ten times smaller than those at the free surface) characterize the surface of the sheet in contact with the drums. The observations in Fig. 3c–f (again couples of photos of the same sheet with a different focal distance each) with sheets produced under other drum speeds are in line with those in Figs. 3a and b, only now craters and bubbles are smaller in size. This is due to the thinner sheets produced at higher drum speeds, an observation also noted by Vallous et al. [31] and Kalogianni et al. [33].

The aforementioned appearance of the produced starch sheets is a result of the boiling-type of drying that occurs in a drum dryer when the humid gelatinized starch in the pool suddenly adheres on the hot drum wall to form a thin film (e.g. [34,35]). At the beginning of drying, steam bubbles created at the lower surface of the sheet (in contact with the drum) escape towards the top (free) surface of the sheet. As the sheet progressively dries along the rotation, the material of the sheet becomes so viscous that cannot pull back

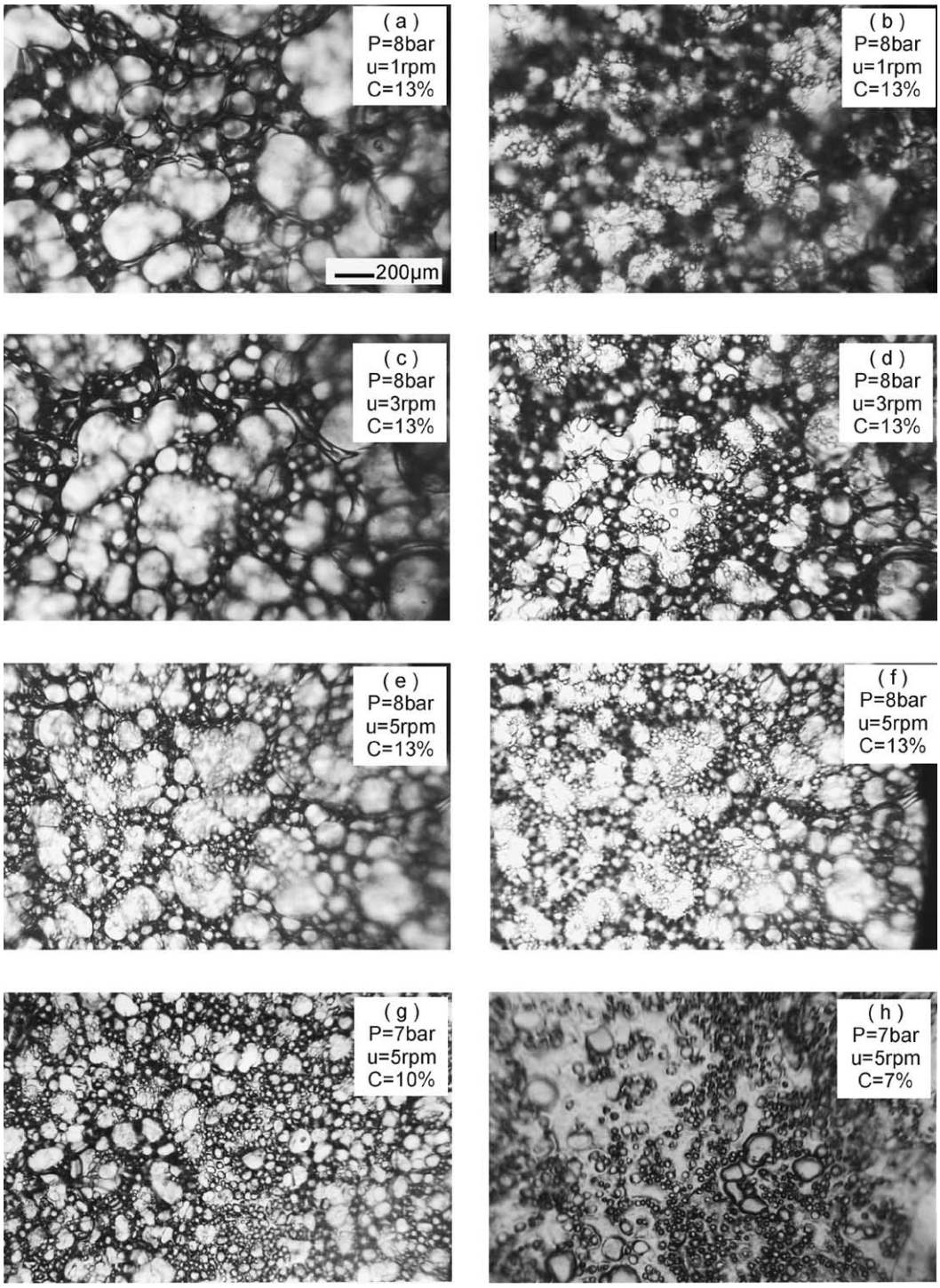

Fig. 3. Microscopy of starch sheets produced at different steam pressure (*P*), drum rotation speed (*u*), and feed concentration (*C*): (a, c, e, g and h) free surface of the sheet; (b, d and f): surface in contact with the drums.

together after the departure of bubbles and so they leave behind vacant spaces which solidify and turn into open craters. Such open craters are clearly observed in Fig. 3a and b. In addition, some of the steam bubbles formed at the end of boiling are trapped in the solid matrix because the outer surface of the sheet is extremely viscous. Inside these bubbles, the steam recondenses upon cooling (air eventually invades by diffusion) and as a result these are the moistest parts of the sheets at the moment of their production.

Sheets produced by 10% starch feed concentration (Fig. 3g) display much smaller craters and bubbles than those of the 13% starch feed concentration since the sheets are now much thinner. This is so despite the lower steam pressure, which in principle yields thicker sheets, and is

because the thickness of the sheets depends more on feed concentration than on rotation speed and steam pressure [33]. As a result, the two sides of the sheet in Fig. 3g (free surface and in contact with the drums) differ less than in Fig. 3a–f. Since the sheet in Fig. 3g is quite thin, the employed optical depth of field is adequate to discern details both at the top and the bottom surface of the sheet. In the sheets produced with 7% starch feed concentration (Fig. 3h), practically no craters exist and the trapped air bubbles are smaller compared to the other two feed concentrations. In those sheets, there is essentially no morphology differentiation between the two sides of the sheets.

3.3. Wicking rates of various alkanes in starch sheets

Fig. 4 shows a representative wicking plot where h^2 versus t curves are displayed for all wicking liquids tested with samples of the same product (drum dryer input variables: starch feed concentration 13%, steam pressure 8 bar, drum speed 5 rpm). In order to demonstrate the effect of the inherent variability in product porosity (which may vary a little among samples of the same product), two curves are presented for some wicking liquids (each curve taken with a different sample). The observed porosity variability, reflected in the varying slopes of the two curves obtained with the same wicking liquid, is definitely over and above experimental errors (manifested as fluctuations within the same curve) and may be attributed, at least in part, to minor differences in product thickness. The two curves represent limiting outmost runs among repetitions and show that despite any porosity fluctuations from one sample to another, the penetration rate still shows a monotonous trend among liquids. The good linear dependence of h^2 on t is in agreement with the Lucas–Washburn equation. No gravity effects are evident in the plots as expected because $h \ll h_{eq}$. A typical length for h_{eq} in decane would be $\sim 6 \times 10^5$ m for a 10 nm diameter capillary and $\sim 6 \times 10^2$ m for a 10 μm diameter capillary. The fastest wicking rate is observed for heptane and drops as the molecular weight of the wicking liquids increases. This is due to the higher rise in viscosity compared to the rise in surface tension of the wicking liquids as their molecular weight increases.

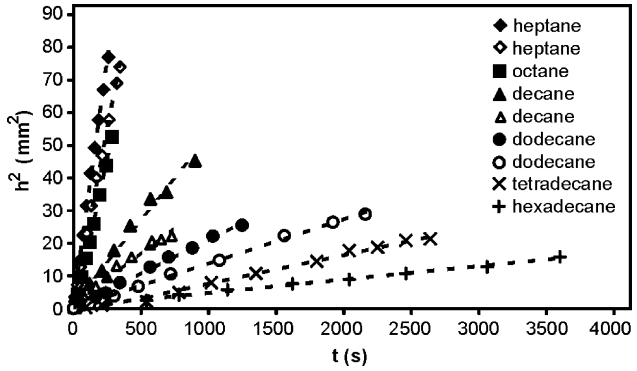

Fig. 4. Wicking rate of various alkanes on a drum dryer modified starch sheet. Drum dryer input variables: starch feed concentration, 13%; steam pressure, 8 bar; drum rotation speed, 5 rpm.

3.4. Determination of the effective pore radius

In Fig. 5a, the type of plot proposed by van Oss et al. [15] for the determination of r is presented. Error bars represent the standard deviation in the determination of each data point including repetitions. The fitting of the data with a straight line passing through the origin is bad and as a result a poor linear regression coefficient is found. The limited spread of γ values in the x-axis together with the appreciable scatter in the data account for the bad fit. van Oss et al. [15] and Li et al. [14], using the same wicking liquids, had also a significant data scatter but due to the larger pores in their samples (~10 μm while ours are ~10 nm, see further) the slope yielding r was greater resulting in better estimation statistics.

An improved way to analyze our data is by plotting $2h^2/t$ versus γ/η (so that the slope remains equal to r), as in Fig. 5b. The data scatter along the fitted line passing through the origin is evidently less than in Fig. 5a while the better scaling along both axes yields higher accuracy in the determination of r. The discrepancy for tetradecane may imply an increasing effect of viscosity over surface tension. Table 2 presents

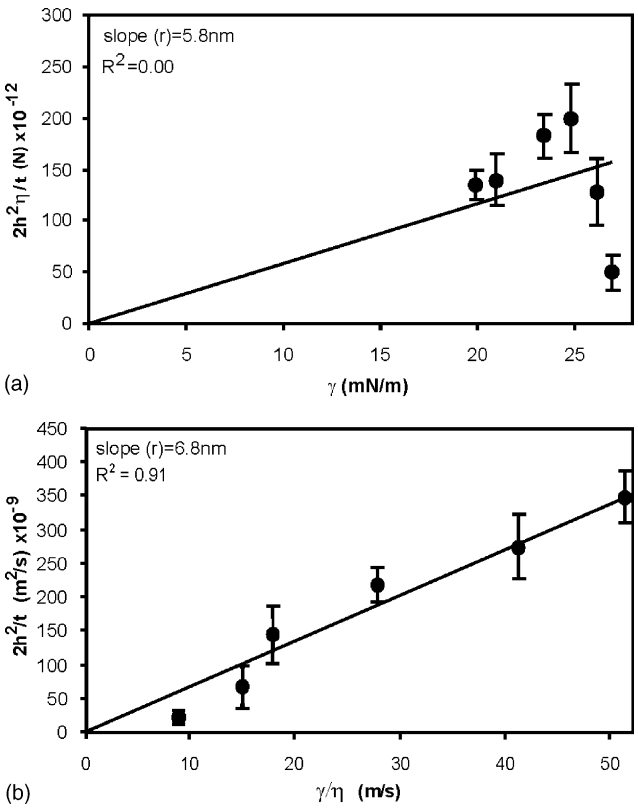

Fig. 5. Plot for the determination of the effective mean pore radius (r): (a) as proposed by van Oss et al. [15]; (b) as used in the present study. Drum dryer input variables: starch feed concentration, 13%; steam pressure, 8 bar; drum rotation speed, 5 rpm. Error bars stand for the standard deviation including repetitions.

Table 2
Effective mean pore radius (r) of starch sheets produced at variable steam pressure (P) drum rotation speed (u) and starch feed concentration (C)

Drum dryer input variables			r_{mean} (nm)	Standard deviation (nm)
P (bar)	u (rpm)	C (%)		
8	1	13	12.6	1.3
8	3	13	10.4	1.3
8	5	13	6.8	0.4
7	5	7	5.9	1.8
7	6	7	3.6	0.6
7	4	13	13.9	2.3
7	5	13	10.3	1.0
7	6	13	8.1	1.3
7	5	10	4.7	1.2

Values of the standard deviation (st. dev.) of the determination are also given.

collectively the results obtained by the latter representation for all products, including the standard deviation of r from all repetitions. Despite the appreciable standard deviation in the computed effective pore radii, it is apparent that different products have different pore sizes depending on the drum dryer's operational conditions. It must be stressed here that with physical products it is not unusual that porosity of the same product can span a broad range of values [9].

3.5. Effect of drum dryer input variables on the sheets effective pore radius

Fig. 6 depicts graphically how the dryer's input variables influence the effective pore radius of the product sheets, as determined by the wicking technique. A tendency for smaller pores is found for increasing drum rotation speed, increasing steam pressure and decreasing starch feed concentration.

In order to get some insight, we cross-examined the present results with the effect of the dryer's input variables on other physical characteristics of the starch sheets, as reported by Vallous et al. [31] and Kalogianni et al. [33]. These authors have worked with the same drum dryer (and range of dryer's input variables), maize starch and feed

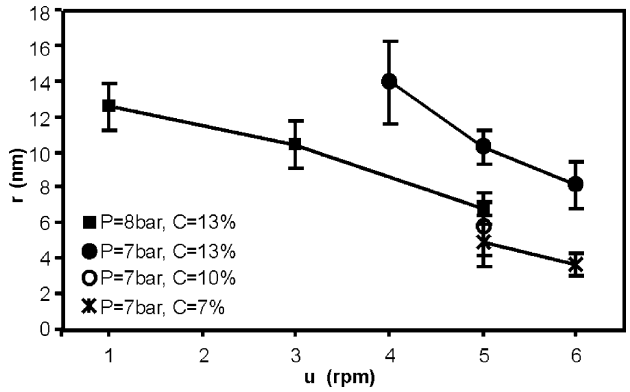

Fig. 6. Effect of drum dryer input variables on the effective mean pore radius (r). Error bars stand for the standard deviation of the determined mean including repetitions.

concentrations. They reported that by rising the drum speed or steam pressure or lowering the starch feed concentration, the amount of material that spreads as a thin film over the drums surface (kg dry mass/m^2) decreases. This quantity (termed as specific load) is roughly equivalent to sheet thickness [31]. Hence, the smaller effective pore radius is encountered in the thinner sheets. Nevertheless, no explanation can be offered at this time whether this is due to the sheet thickness alone or other sheet properties as well (rheological, thermophysical, etc.).

The variation of the effective pore radius among products determined by the wicking technique agrees qualitatively with the observations made by optical microscopy (Fig. 3). However, the pores determined by wicking are much smaller in size. These smaller pores could not be resolved by optical microscopy. Moreover, microscopy gives no safe information on whether the observed large cavities are interconnected (forming a network) or not. The wicking results demonstrate that hydration of the internal porous matrix of the drum sheets is governed not by the large cavities observed by microscopy, $O(\sim 100\,\mu m)$, but from the smaller pores, $O(\sim 10\,nm)$, that compose a network at the bottom side of the sheets (in contact with the drum surface). Regarding their commercial application, the produced pregelatinized starch sheets are further ground milled to become a thin powder, with a mean grain diameter of less than $\sim 300\,\mu m$, and as such are made available to end users (for rehydration). During milling, cavities with diameters of the order of 10–100 μm may be largely destroyed while pores extending only a few nm remain practically unaffected. These smaller pores are expected to control the hydration of the powder.

3.6. Conditions for the application of the wicking technique: the case of porous foods

When using the Lucas–Washburn equation for the determination of pore radius, a question arises regarding the value of $\cos\theta$. The use of alkanes provides that $\cos\theta = 1$ at equilibrium (static) conditions but it is doubtful whether the contact angle remains equal to zero at dynamic (advancing) conditions, thus during wicking. In principle, the value of the advancing contact angle is higher than the equilibrium contact angle [36] and departs more and more from the equilibrium value as the velocity of the liquid increases [24]. If this effect is not taken into account, it can cause serious underestimation of the effective pore radius. Since the dynamic contact angle cannot be measured directly in porous media, Siebold et al. [24] proposed an alternative treatment of the wicking data where $r\cos\theta$ (as calculated by the Lucas–Washburn equation) is plotted against the initial velocity of penetration, $v = h/t$, of the different liquids. If there is an effect of the advancing contact angle then $r\cos\theta$ will be smaller for higher penetration rates and then only extrapolation to zero velocity (so that $\cos\theta = 1$) can give the actual effective pore radius of the medium. Applying the

analysis of Siebold et al. [24] to our data showed no influence of the advancing contact angle.

In another relevant study, Sedev et al. [37] showed that for liquid velocities lower than 0.15 mm/s, there was virtually no dependence of the advancing contact angle (of octane and hexadecane on FC-722 coated mica) on liquid velocity. The advancing contact angle for such velocities was equal to the static one. Alkane velocities in our study never exceeded 0.10 mm/s even at the very beginning of wetting. Apart from that, Marmur [38] argued that if the Lucas–Washburn equation is respected, i.e. h^2 versus t is linear, contact angle dynamic effects can be safely ignored. In our experiments the linear regression coefficient (R^2) of the fitted lines, i.e. in Fig. 4, was better than 0.95.

The aforementioned researchers conducted their experiments on one specimen (more or less the same in all runs), often tailor-made to have a smooth solid surface. On the contrary, with foods it is not possible to use repeatedly the same specimen in successive wetting–dewetting runs, since the product's quality gets highly demoted. So when working with foods, one has to assure reproducibility among different samples of the same product in order to obtain statistically significant results. In addition, food porous media are characterized by considerable inherent roughness. Roughness tends to diminish the value of the apparent contact angle for liquids spontaneously wetting a solid ($\theta < 90^\circ$) [39]. This is the case for the alkanes used here. All the above support the notion that the dynamic contact angles during the present wicking experiments were sufficiently close to zero.

Another point that should be stressed is the importance of saturating the porous matrix with vapors of the liquid before the wicking experiment. In the words of Good [23], "if a porous body is initially devoid of any absorbed film of the liquid that penetrates it and if molecules of the fluid are not transported ahead of the liquid front by diffusion, the rate of penetration will be faster than predicted by the Lucas–Washburn equation." In this case, the Lucas–Washburn equation should be modified by the addition of the spreading pressure of the film transported ahead the liquid. Values of the spreading pressure are scarce in literature but some values reported for alkanes by Adamson and Gast [39] are very low. Therefore, in products like the sheets tested here, fluctuations due to the inherent variability in pore sizes may be over and above (and may mask entirely) the probable effect of spreading pressure.

The meticulous experiments of Chibowski and Holysz [16,17], on thin layer inorganic powders, verified the theoretical arguments of Good [23] for low molecular weight (volatile) alkanes (hexane, heptane, octane) although for dodecane (practically not volatile at ambient conditions) no differences were found. Daillant et al. [40] using X-ray reflectivity showed that even with non-volatile spreading liquids of high viscosity such as siloxane oil (siloxane oil had much higher viscosity than hexadecane and a surface tension around 20 mN/m), a precursor film precedes the penetrating liquid front.

Table 3
Effect of contact time with tetradecane vapors on the wicking rate (h^2/t) of starch sheets

Contact time with tetradecane vapors	Wicking rate (mean ± S.D., mm^2/s)
0 h (22 °C)	0.068 ± 0.008
24 h (22 °C)	0.071 ± 0.009
6 Days (45 °C)	0.069 ± 0.005

Drum dryer input variables: starch feed concentration, 13%; steam pressure, 8 bar; drum rotation speed, 1 rpm.

Although the liquids used in our study were the same as in van Oss et al. [15], it was considered important to check here for possible partial saturation of the porous matrix of the starch sheets. It was beyond doubt that the low molecular weight alkanes (heptane, octane) would form an absorbent film due to their high volatility and the fact that they were left prior to measurement in the closed glass box together with the sample until saturation (see Section 2). However, the performance of the higher molecular weight alkanes, being practically non-volatile at ambient temperature, was a matter of concern. A few tests were made with tetradecane. Just before wicking, the samples were left for saturation in the closed test box together with tetradecane while the saturation period and temperature were varied, as presented in Table 3. All three experiments showed approximately the same mean wicking rate (integrated over the entire wicking period). It might be possible therefore that a precursor film was also present in our case, resulting in no effect of saturation time and temperature on wicking rate. Perhaps, this is due to the inherent roughness and disorder of a food porous network, which retards the motion of the penetrating front around the local defects, leaving thus more time for such a precursor film to emerge.

An alternative version to the dynamic wicking technique used here is the equilibrium wicking technique, sometimes called the Bartel method. This actually relates the equilibrium capillary rise inside a porous medium with a hydrostatic or a pressure driving force to determine the effective pore radius (e.g. [41–43]). This version of the technique is practically inapplicable to food items since it usually requires a considerable sample height and an appreciable long time to reach the final equilibrium height, especially when the food pores are of the order of nanometers. Marmur and Cohen [44] reported an intermediate between the two versions. Their technique is dynamic, in the sense that it describes the kinetics of wicking by a new mathematical analysis but requires an adequate wicking length so that gravity effects can play a definitive role, yet far enough from the final equilibrium height. For samples having an effective pore radius of 10 nm being wicked with heptane, this technique needs at least 4 m of penetration length in able to perform a reliable data analysis (calculations are made by the equations provided by Marmur and Cohen [44]). This is experimentally very difficult to handle and, apparently, it is not possible with our samples. However, for samples characterized by a

10 μm effective pore radius the required wicking height is a little more than 1 cm and wicking with heptane lasts only about 10 min, making the experiment feasible. Perhaps, the most interesting feature in the analysis of Marmur and Cohen [44] is that it can yield a distribution of effective pore radii if just a single pore radius value fails to characterize the porous structure of the material.

4. Conclusions

A dynamic wicking technique has been employed with considerable success for the determination of the effective mean pore radius of drum dried pregelatinized starch sheets. The technique is fast and easy to perform, attributes very important for delicate thin-layer food items (such as the drum dryer sheets tested here) where measurement by other techniques (i.e. mercury intrusion porosimetry) is difficult to perform. The determined effective mean pore radius of the examined starch sheets varied from ∼4 to 14 nm. Lower drum rotation speeds, lower steam pressures and higher starch feed concentrations tend to give products characterized by larger pores. These results are important for the further development of drum dried products. The possible influence of dynamic contact angle effects in the observed wicking rates has been examined thoroughly. Such effects, experienced by other authors when working with single glass capillaries and inorganic porous media, were not detected in our experiments. This is rather due to the employed low wicking velocities combined with the considerable inherent roughness of the starch sheets. The probable dependence of the wicking rates on the partial saturation of the porous matrix with vapors of the liquid has been another matter of concern. It appears that this effect—if it exists at all—is less than the effect of the inherent variability of pore sizes inside the same piece of sheet (as a result of the intense drying process occurring over the drums), and so it is completely masked.

References

[1] S.N. Marousis, V. Karathanos, G.D. Saravacos, J. Food Process. Preserv. 15 (1991) 183.
[2] X. Xiong, G. Narsimhan, M.R. Okos, J. Food Eng. 15 (1991) 187.
[3] M.S. Rahman, O.S. Al-Amri, I.M. Al-Bulushi, J. Food Eng. 53 (2002) 301.
[4] G. Jeronimidis, in: J.M.V. Blanshard, J.R. Mitchell (Eds.), Food Structure—It's Creation and Evaluation, Butterworths, London, 1988 (Chapter 5).
[5] S.N. Marousis, G.D. Saravacos, J. Food Sci. 55 (5) (1990) 1367.
[6] V.T. Karathanos, N.K. Kanellopoulos, V.G. Belessiotis, J. Food Eng. 29 (1996) 167.
[7] J.M. del Valle, V. Aránguiz, L. Diaz, J. Food Eng. 38 (1998) 207.
[8] S. Hogenkamp, M. Pohl, Powder Technol. 130 (2003) 385.
[9] A.H. Barret, E.W. Ross, J. Food Sci. 55 (1990) 1378.
[10] D.K. Rassis, I.S. Saguy, A. Nussinovitch, Food Hydrocolloids 16 (2002) 139.
[11] C. Zhao, X. Zhou, Y. Yue, Desalination 129 (2000) 107.
[12] V. Karathanos, S. Anglea, M. Karel, Drying Technol. 11 (1993) 1005.
[13] V.T. Karathanos, G.D. Saravacos, J. Food Eng. 18 (1993) 259.
[14] Z. Li, R.F. Giese, C.J. van Oss, K.M. Kerch, H.E. Burdette, J. Am. Ceram. Soc. 77 (1994) 2220.
[15] C.J. van Oss, R.F. Giese, Z. Li, K. Murphy, J. Norris, M.K. Chaudhury, R.J. Good, J. Adhes. Sci. Technol. 6 (1992) 413.
[16] E. Chibowski, L. Holysz, Langmuir 8 (1992) 710.
[17] L. Holysz, E. Chibowski, Langmuir 8 (1992) 717.
[18] Z. Li, R.F. Giese, C.J. van Oss, J. Yvon, J. Cases, J. Colloid Interface Sci. 156 (1993) 279.
[19] P.M. Costanzo, W. Wu, R.F. Giese Jr., C.J. van Oss, Langmuir 11 (1995) 1827.
[20] W. Wu, R.F. Giese, C.J. van Oss, Powder Technol. 89 (1996) 129.
[21] E.W. Washburn, Phys. Rev. 17 (1921) 273.
[22] L.R. Fisher, P.D. Lark, J. Colloid Interface Sci. 69 (1979) 486.
[23] R.J. Good, J. Colloid Interface Sci. 42 (1973) 473.
[24] A. Siebold, M. Nardin, J. Schultz, A. Walliser, M. Oppliger, Colloids Surf. A: Physicochem. Eng. Aspects 161 (2000) 81.
[25] B.V. Zhmud, F. Tiberg, K. Hallstensson, J. Colloid Interface Sci. 228 (2000) 263.
[26] G. Matic, J. De Coninck, T.D. Blake, J. Colloid Interface Sci. 263 (2003) 213.
[27] S. Hodge, M. Osman, in: O.R. Fennema (Ed.), Food Chemistry. Principles of Food Science (Part 1), Marcel Dekker, New York, 1976 (Chapter 5).
[28] P. Collona, A. Buleo, C. Mercier, in: T. Galliard (Ed.), Starch: Properties and Potential, Critical Reports on Applied Chemistry, vol. 13, Wiley, New York, 1987 (Chapter 5).
[29] D.R. Lide (Ed.), Handbook of Chemistry and Physics, 79th ed., The Chemical Rubber Co., Cleveland, 1988.
[30] G. Rodriguez, J. Vasseur, F. Courtois, J. Food Eng. 28 (1996) 271.
[31] N.A. Vallous, M.A. Gavrielidou, T.D. Karapantsios, M. Kostoglou, J. Food Eng. 51 (2002) 171.
[32] A. Anastasiades, S. Thanou, D. Loulis, D. Stapatoris, T.D. Karapantsios, J. Food Eng. 52 (2002) 57.
[33] E.P. Kalogianni, V.A. Xynogalos, T.D. Karapantsios, M. Kostoglou, Lebensm. Wiss. Technol. 35 (2002) 703.
[34] J. Vasseur, F. Abchir, G. Trystram, in: A.S. Mujumdar, I. Filkova (Eds.), Drying '91, Proceedings of the Seventh International Drying Symposium, Prague, 26–30 August 1990, Elsevier, New York, 1991, p. 121.
[35] M.A. Gavrielidou, N.A. Vallous, N.A. Karapantsios, J. Food Eng. 54 (2002) 45.
[36] P.G. de Gennes, Rev. Mod. Phys. 57 (1985) 827.
[37] R.V. Sedev, C.J. Budziak, J.G. Petrov, W. Neumann, J. Colloid Interface Sci. 159 (1993) 392.
[38] A. Marmur, Langmuir 19 (2003) 5956.
[39] A.W. Adamson, A.P. Gast, Physical Chemistry of Surfaces, sixth ed., Wiley, New York, 1996.
[40] J. Daillant, J.J. Benattar, L. Leger, Phys. Rev. A 41 (1990) 41.
[41] L.R. White, J. Colloid Interface Sci. 90 (1982) 536.
[42] D. Dunstan, L.R. White, J. Colloid Interface Sci. 111 (1986) 60.
[43] D. Diggins, L.G.J. Fokking, J. Ralston, Colloids Surf. 44 (1990) 299.
[44] A. Marmur, R.D. Cohen, J. Colloid Interface Sci. 189 (1997) 299.